RESEARCH ARTICLE | JULY 10 2023

De-wetting of evaporating drops on regular patterns of triangular posts

Hsuan-Yi Peng [ID] ; Bang-Yan Liu [ID] ; Chi-Chun Lo; Li-Jen Chen [ID] ; Ralf Seemann [ID] ; Martin Brinkmann [✉] [ID]

Check for updates

View Online

Export Citation

CrossMark

AIP Publishing

De-wetting of evaporating drops on regular patterns of triangular posts

View Online   Export Citation   CrossMark

Hsuan-Yi Peng,[1] (iD) Bang-Yan Liu,[1] (iD) Chi-Chun Lo,[1] Li-Jen Chen,[1] (iD) Ralf Seemann,[2] (iD) and Martin Brinkmann[2,a)] (iD)

AFFILIATIONS

[1] Department of Chemical Engineering, National Taiwan University, 10617 Taipei, Taiwan
[2] Experimental Physics and Center of Biophysics, Saarland University, 66123 Saarbrücken, Germany

Note: This paper is part of the JCP Special Topic on Chemical Physics of Controlled Wettability and Super Surfaces.
[a)] Author to whom correspondence should be addressed: martin.brinkmann@physik.uni-saarland.de

ABSTRACT

Directional wicking and spreading of liquids can be achieved by regular micro-patterns of specifically designed topographic features that break the reflection symmetry of the underlying pattern. The present study aims to understand the formation and stability of wetting films during the evaporation of volatile liquid drops on surfaces with a micro-pattern of triangular posts arranged in a rectangular lattice. Depending on the density and aspect ratio of the posts, we observe either spherical-cap shaped drops with a mobile three-phase contact line or the formation of circular or angular drops with a pinned three-phase contact line. Drops of the latter class eventually evolve into a liquid film extending to the initial footprint of the drop and a shrinking cap-shaped drop sitting on the film. The drop evolution is controlled by the density and aspect ratio of the posts, while no influence of the orientation of the triangular posts on the contact line mobility becomes evident. Our experiments corroborate previous results of systematic numerical energy minimization, predicting that conditions for a spontaneous retraction of a wicking liquid film depend weakly on the orientation of the film edge relative to the micro-pattern.

I. INTRODUCTION

Spontaneous wicking of porous materials by wetting liquids is a well-known phenomenon encountered in our daily lives.[1] Examples include water drawn up into a dry sponge[2] or a piece of paper,[3] and ink flowing into the nib of a pen by capillary action.[4] Spreading and imbibition of liquids are also observed on rough surfaces,[5] whose wicking abilities are closely linked to the interplay between surface geometry and surface energies.[6] Surfaces equipped with dense structures with high aspect ratio topographies promote spontaneous wicking of wetting liquids, provided the density and slope of the surface features are sufficiently high.[7] Wrinkles and ridges found on human skin are examples of topographic features that facilitate liquid spreading on a rough surface.[8]

Periodic micro-patterns of posts with a square or circular cross section are widely used as model systems to study the spreading and wicking of liquids on non-flat surfaces due to the relatively simple fabrication of micrometer-sized structures by photolithography.[7,9–13] Owing to the discrete lattice symmetries, a strong

faceting of the wicking liquid film is observed if the density of posts exceeds a certain value. This anisotropic film spreading can be related to the sensitivity of the dynamics of interfacial advance with respect to the orientation of the film edge relative to a micro-pattern.[11,12] It is predicted that the normal vectors of the facets point in the directions of the slowest advance.[12]

Surface features breaking the reflection symmetry of the micro-pattern potentially give rise to a preference for wicking in certain directions over the respective opposite direction. Such directional wicking of liquids has been experimentally realized, e.g., in dense arrays of high aspect ratio posts that collectively bend into one direction[14] and in open micro-channels equipped with fishbone-like or more complex features allowing the liquid to progress in only one direction.[15,16] Chemical modification of certain parts of the surface can also be employed to generate uni-, bi-, and tri-directional wicking in micro-patterns of topographic features that conform to the reflection symmetry of the underlying lattice.[17,18] Directional wicking in periodic arrays of posts with triangular cross section has been studied in wetting experiments,[19,20] in simulations,[21,22] and in

15 November 2023 08:47:43

numerical energy minimizations.[20] An example of a topographic structure that promotes directional wicking in nature is the skin of the Texas horned lizard.[23]

Several studies derive necessary conditions for liquid wicking on micro-patterned surfaces from simple thermodynamic considerations.[7] In their approach, the interfacial energy of the wicking film and of the dry surface structure are compared and the state of lower energy determines whether a liquid film in contact with a liquid reservoir spontaneously advances into the micro-pattern or whether it recedes from it.[7] However, due to this coarse-grained approach, thermodynamic considerations of global energy minima cannot explain anisotropic and directional wetting phenomena, including the faceting of wicking liquid films found in the periodic arrangement of posts. Because of their simplicity, thermodynamic arguments do not account for the possibility that a liquid interface at the edge of the film is trapped in one of the numerous local energy minima.[20,24] Those metastable states of the interface can cause an arrest of the liquid film edge, even if the interfacial energies averaged over length scales larger than the typical dimensions of the topographies would allow wicking or de-wicking of the liquid.[20,24]

In the present work, we consider the de-wetting of evaporating drops on surfaces with micro-patterns of triangular posts employed in a previous study on directional wicking.[20] Directional wicking and de-wicking of liquid films in a periodic lattice of triangular posts can be understood from the morphology of the interface close to the three-phase contact line and the mechanisms that lead to interfacial advance on the length-scale of the posts.[20] In a certain range of density and aspect ratio of the posts, the orientation of a film edge relative to the micro-pattern determines whether the film advances, recedes, or is arrested.

So far, it has not been clarified whether the broken reflection symmetry of this class of micro-patterns manifests in a directional dependence of the mobility of the interface observed during a receding motion of the liquid. Predictions of the range of post densities and aspect ratios allowing the film to recede obtained in Ref. 20 by numerical energy minimizations have not been tested in experiments and are addressed in this article.

II. METHODS

A. Experimental

Conditions for the formation and stability of liquid films during de-wetting are systematically studied in experiments on surfaces decorated with a periodic pattern of triangular posts breaking the reflection symmetry of the underlying lattice; cf. the sketches in Figs. 1(a) and 1(b). All types of surfaces tested in the present work have been employed in previous research on the reverse situation of directional wicking of liquid films.[20]

As shown in Figs. 1(a) and 1(b), the micro-patterned surfaces used in our experiments consist of periodically arranged posts with a uniform height h and a homogeneous equilateral triangular cross section. The aspect ratio of the posts is specified by the ratio $AR = h/w$ with the base-width of a triangle, $w = (18.5 \pm 0.5) \, \mu m$ for all fabricated pattern geometries. The posts are arranged such that the base of the triangles is aligned with the long side of the rectangular unit cell. The ratio r/d of the periodicities r in the y-direction (tip direction) and d in the x-direction (side direction) is taken to be identical to the ratio between the height of the triangle, a, and
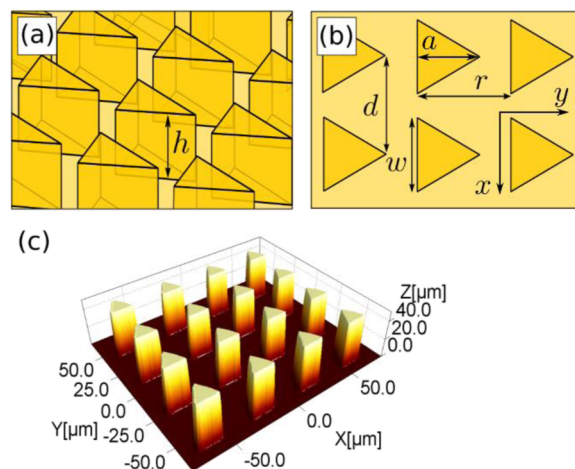

FIG. 1. (a) and (b): Illustration of the topographic micro-pattern of equilateral triangular posts used in our de-wetting experiments. Periodicities in the y- and x-directions are set to the ratio $r/d = a/w = \sqrt{3}/2$, such that the post density is fixed by the line fraction $LF = w/d$ of posts. The aspect ratio $AR = h/w$ of the posts is the ratio of post height h to base width w. (c): White-light interferometry image of a micro-patterned surface used in the experiments.

the base w, i.e., $r/d = a/w = \sqrt{3}/2$, cf. Fig. 1(b). A uniform scaling of the spatial periods of the post array into x- and y-directions while keeping the dimension of the posts' constant leads to micro-patterns with variable post densities but with identical line fractions when projected in the x- and y-directions, respectively. Hence, the geometry of each micro-patterned surface is uniquely characterized by the line fraction $LF = w/d$ of the posts and their aspect ratio $AR = h/w$.

Samples for various combinations of line fractions and aspect ratios of the posts were fabricated in SU8 photoresist using standard photolithography techniques. First, a layer of SU8 photoresist (Kayaku Advanced Materials, Inc., MA, USA) is spin-coated onto a plane glass surface to form a film of uniform thickness. The film is then exposed to UV light through a chromium mask with periodic arrays of triangles. After post-exposure baking, the SU8 layer is developed to obtain arrays of freestanding posts of photo-resin with the desired triangular cross section. Micro-patterns with different geometries are achieved by varying the thickness of the SU8 layer and the periodicity of the triangles. To modify the wettability of the samples and to obtain a chemically resistant and chemically homogeneous surface, the glass with the SU8 pattern is coated with a thin Teflon layer (Teflon AF 1061S, DuPont). A final characterization of the fabricated micro-patterns was done by optical microscopy (Olympus, BXFM) and by confocal microscopy (KEYENCE, VK-X210), cf. Fig. 1(c). For more details about our sample fabrication and characterization, we refer the reader to Ref. 20.

In all experiments, heptane was used as a test liquid with an advancing contact angle of $\theta_a = (51.6 \pm 1.0)°$ and a receding contact angle of $\theta_r = (42.7 \pm 1.2)°$. Employing the embedded needle technique,[25] both contact angles were measured on a flat Teflon-coated SU8 reference surface using a home-made goniometer set-up for enhanced video-microscopy in combination with numerical analysis tools.[26] To study the shape evolution of sessile liquid drops

on a micro-patterned surface, a pendant drop of about 3 μl heptane was gently deposited on the surface from the tip of a hollow steel needle. An optical reflecting microscope in the top view was employed to record the shape evolution of the liquid interface during evaporation.

B. Numerical modeling

In a previous study, the morphology and stability of liquid films in a micro-pattern of triangular posts were studied using numerical minimizations of the interfacial energy[20] As we show in this study, the numerical results are not only applicable to derive conditions for directional wicking but also to predict whether a liquid film spontaneously de-wicks from a given pattern geometry. In the following, we will provide the reader with relevant details of the numerical modeling.

To study the equilibrium morphology and stability of the film interface in contact with the micro-pattern, we performed systematic energy minimizations using the free software Surface Evolver.[27] In the approach of the Surface Evolver, the liquid–air interface is represented as a mesh of small triangles. This interface is bounded by the three-phase contact line where the liquid–air interface meets the solid. Specific wetting geometries, such as posts with a certain homogeneous cross section, are implemented in the form of local constraints that are applied to the vertices and edges of the mesh, representing different parts of the three-phase contact line.[20,24,28] The latter constraints force the vertices of the three-phase contact line to remain on specific parts of the solid surface. For every configuration of the liquid–air interface, as given by the position of all vertices, the contribution of the wet surface to the total interfacial energy is computed from the position of the three-phase contact line. The contribution of the liquid–air interface of the model interface to the total interfacial energy is computed from the sum of the areas of all triangles. To conform to the experimental situation, we assume that the film exchanges volume with a liquid reservoir representing the drop. Because the Laplace pressure is fixed, no global constraint on the liquid volume in the film is necessary for our model. In this Laplace pressure-controlled ensemble, the pressure difference between liquid and air is fixed, and the total energy to be minimized must contain a term that accounts for the work done at the reservoir. In modeling the present experimental situation, this term vanishes because the Laplace pressure is zero on the scale of pressures given by the ratio of interfacial tension to the typical length scale of the micro-pattern.

To assess the mechanical stability of the interface close to the edge of the post structures, we considered only a section of the liquid film in our numerical model. Owing to the expected discrete symmetries of the interface shape in mechanical equilibrium, we could restrict the model interface to an elongated rectangular stripe with periodic boundary conditions applied in the direction parallel to the film edge, or to even one-half of the periodic stripe if the configurations are expected to exhibit a reflection symmetry perpendicular to the film edge. Since the liquid–air interface for a vanishing Laplace pressure flattens out quickly as one moves away from the terminal three-phase contact line, it is sufficient to consider only three or four rows of posts in contact with the film behind the terminal meniscus. In addition, the boundary conditions at the side of the stripe, the liquid–air interface of our model is subject to a local constraint at the short side of the stripe, opposite to the film edge. Here, a virtual vertical wall of neutral wettability enforces the mirror symmetry of the interface. This constraint allows the free interface to move up and down and to adjust to global changes in the film morphology. Alternatively, we fixed the height of the interface on the short side to the height of the post. Comparing the results between the neutral wall and fixed boundary conditions showed only minor differences in terms of the interfacial configuration and energy, corroborating the rapid damping of interface deformations caused by the presence of the film edge at distances greater than a few rows of posts.

Posts in the interior of the film are completely engulfed by liquid, while posts in the terminal row at the film edge may be only in partial contact with the liquid. To account for this degree of freedom, we used a series of numerical models of the interface differing in the interface morphology at the terminal meniscus, including the number of side walls of the posts that are in contact with the liquid. We monitored the position of the three-phase contact line at the base of the posts or the distance of the contact line from the nearest posts to detect whether the actual numerical model of the interface is still consistent with the assumed liquid morphology.

III. RESULTS AND DISCUSSION

First, we will describe the morphological evolution of drops on micro-patterned surfaces with triangular posts during evaporation in Sec. III A. The following Sec. III B summarizes results of numerical energy minimizations to determine the stability of the film edge with respect to a receding motion. The experimental findings will then be discussed in light of the stability conditions of a straight liquid film edge with respect to a receding motion in Sec. III C.

A. Morphology evolution of evaporating drops

After deposition on the micro-patterned surfaces, small drops of liquid heptane undergo a series of shape transitions during evaporation, as shown in the sequence of images in Fig. 2. Due to the high vapor pressure of heptane at room temperature when compared to water, the evaporation process of a 3 μl drop does not take longer than about three minutes. In accordance with the findings in our previous work Ref. 20, all pattern geometries tested in the present work do not spontaneously wick heptane drops, as the line fractions and aspect ratios of the micro-patterns fall into the range where no spontaneous wicking is reported in Ref. 20.

1. Early time

Immediately after deposition of the heptane drops on the micro-structured surfaces, clear differences in the drop shape become apparent. Spherical cap-shaped drops with a circular contact line are found on pattern geometries 1, 2, 7, 12, 15a, and 15b with low post densities or small aspect ratios, cf. Fig. 2. However, on sample geometries with dense and tall posts, we observe drops with a polygonal footprint. Drops with octagonal and rectangular footprints can be seen on several pattern geometries in Fig. 2, e.g., on geometries 5 and 6. On the pattern geometries 6, 10, and 11 in Fig. 2, a wicking film with a sharp 90° bend extending from the drop base is visible, cf. also the images in Fig. 3. However, in contrast to the pattern geometries where spontaneous wicking has been reported in Ref. 20, the edge of the wicking film does not detach completely
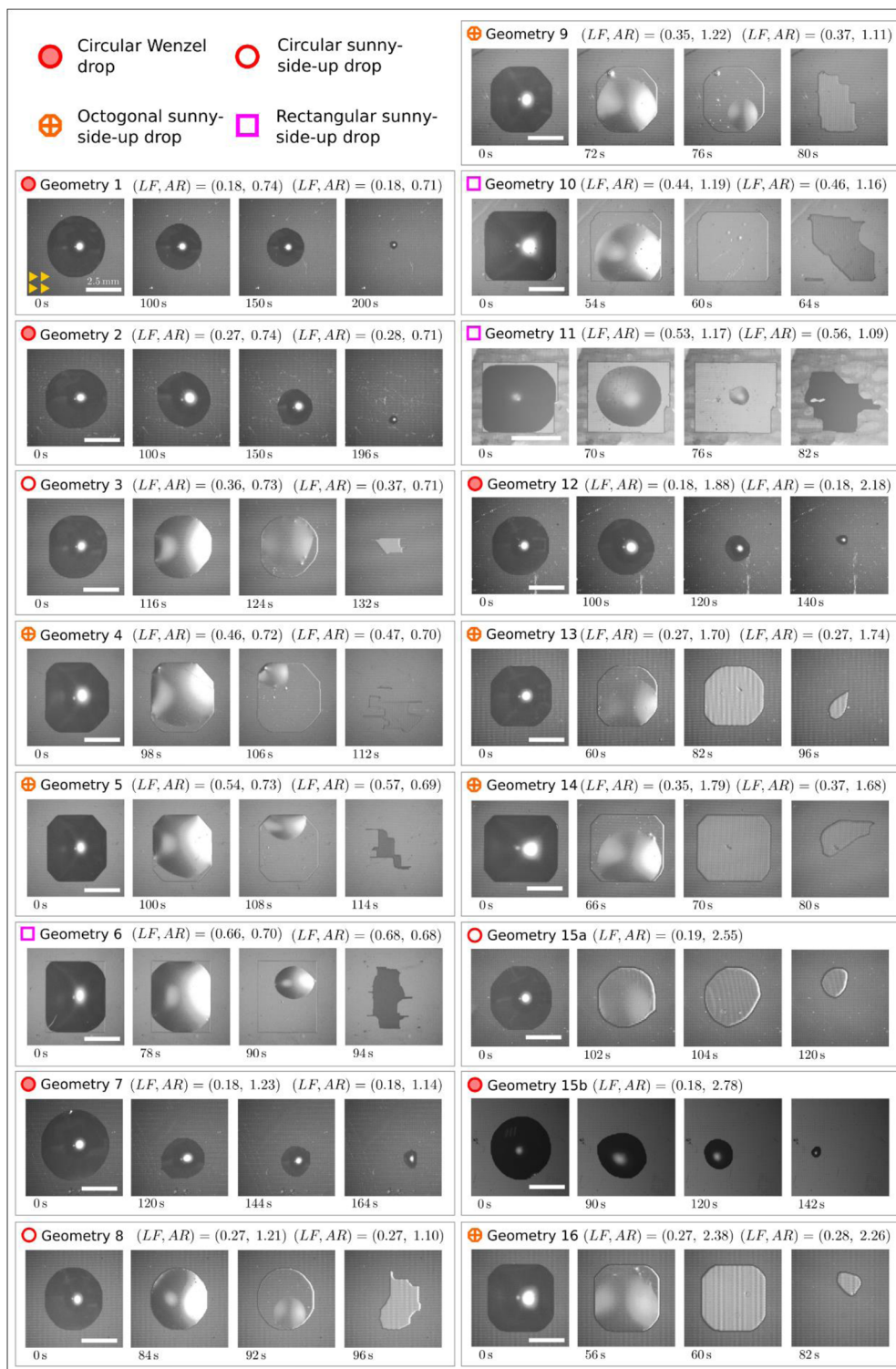
FIG. 2. Morphology evolution of evaporating heptane drops with a volume of 3 μl deposited on a micro-pattern of triangular posts with line fractions $LF = w/d$ and aspect ratio $AR = h/w$. As indicated for geometry 1, the tip direction of the micro-pattern is always to the right, and the base direction is to the left of the image. Symbols indicate the four morphologies observed on the tested pattern geometries. Closed circles: Wenzel drops, open circles: circular sunny-side-up drops, plus/octagon: octagonal sunny-side-up drops, and open square: rectangular and mixed rectangular/octagonal sunny-side-up drops. The scale bar represents 2.5 mm.
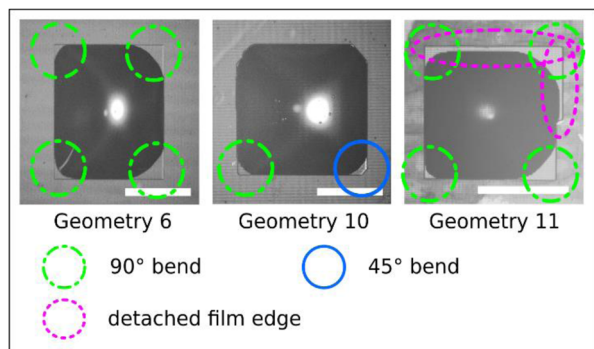
15 November 2023 08:47:43

FIG. 3. Comparison of drops shapes with a rectangular or mixed rectangular/octagonal footprint displaying an extending film already at the time of deposition. All three drops eventually evolve into a sunny-side-up drop. The scale bar represents 2.5 mm.

FIG. 4. Schematic illustration of (a) a Wenzel drop and (b) a sunny-side-up drop found on the regular pattern of triangular micro-posts in our de-wetting experiments.

from the drop base. Only for drops deposited on pattern geometry 11, a detachment occurs in two out of four film orientations. However, all four film edges on this pattern geometry are arrested at a distance of a few rows of posts, indicating that the detachment of the film edge from the drop base is likely due to the kinetic energy of the drop imparted during the deposition process. Similar to all other studied pattern geometries, we could not resolve the drop deposition dynamics leading to the initial shape with the framerate of the camera employed in our experiments. Hence, the contour of the drop base and of the extending film must be attained within a short time interval, not longer than a few microseconds.

2. Intermediate time

During the following liquid evaporation and the concomitant volume loss, the drop morphologies evolve in specific ways. Similar to the early time regime immediately after drop deposition, clear differences in the evolution become apparent between drops wetting pattern geometries with low line fractions or low aspect ratios and drops in contact with surface geometries with high line fractions and high aspect ratios.

Drops with a spherical-cap shape retaining their circular shape throughout the entire evaporation process are found on the pattern geometries 1, 2, 7, 12, and 15b, cf. Fig. 2. The contact line of the latter drops is not pinned to the micro-pattern, which allows the drop base to shrink uniformly. This is an indication that the mobility of the three-phase contact line is insensitive to the local orientation with respect to the underlying micro-pattern. We will speak of "Wenzel drops" because no liquid film is shed as the interface moves across the micro-pattern[10] while the liquid is supposedly in full contact with the surface, cf. the illustration in Fig. 4(a). Slight deviations of the drop base from an ideal circular shape are apparent for, e.g., the drop on pattern geometry 2 shown in Fig. 2, where only part of the contact line of the drop at the lower side in the image is pinned. This asymmetric pinning may lead to the observed lateral motion of the drop center during evaporation.

For drops on pattern geometries with high aspect ratio posts and high line fractions, we observe several features during evaporation that differ qualitatively from the evolution of Wenzel drops.
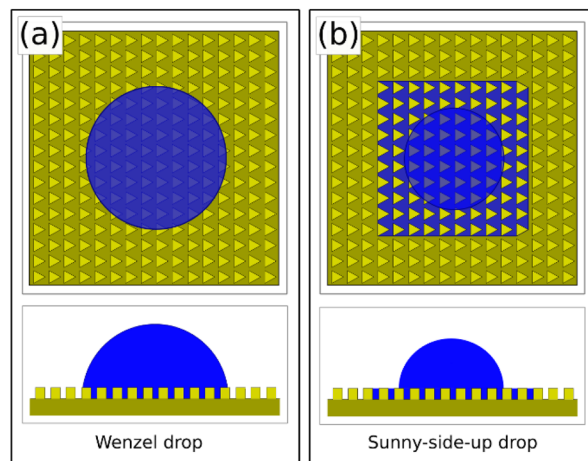
Most strikingly, the three-phase contact line of a drop on these pattern geometries does not recede from its position immediately after liquid deposition. As the drops lose volume during evaporation, the interface first flattens until the drops enter a "sunny-side-up state."[29] In the drop morphology sketched in Fig. 4(b), an almost spherical cap-shaped drop sits atop a liquid film wicking the micro-pattern. The contour of the wicking liquid film is identical to the initial footprint of the drop. The cap-shaped region forming the "egg-yolk" of this drop morphology further shrinks and finally disappears.[29] As the optical contrast of the film in the sunny-side-up state does not change while the egg-yolk drop is shrinking, we assume that the liquid fills the interstice of the micro-pattern up to the level of the top faces of the posts. At the end of this process, immediately after the egg-yolk drop has vanished, the contour of the film edge is still identical to the initial footprint of the drop. In all pattern geometries studied in this work, drops with an initially angular footprint eventually evolve into a sunny-side-up state. However, not all drops with a circular footprint are Wenzel drops, as some drops evolve into the sunny-side-up morphology, cf. the drops on pattern geometry 3 and 15a in Fig. 2.

Inspection of the image series of drops on pattern geometries 3, 4, 5, and 6 in Fig. 5 for similar aspect ratios of posts shows that the apparent contact angle of the egg-yolk drops sitting on top of the film increases with an increasing line fraction. A dependence of the apparent contact angle on the aspect ratio of the post is not visible for egg-yolk drops on pattern geometries 3, 9, and 14 in Fig. 5, with about equal line fractions of triangular posts but increasing aspect ratios.

In view of the mostly irregular shape of the drops, a quantification in terms of the apparent contact angle of the egg-yolk drop on the wicking film was not feasible in our experiments. The qualitative trend, however, is in line with the predictions of the Cassie model for apparent contact angles of sessile drops wetting a chemically heterogeneous and plane surface.[30,31] The Cassie model is applicable to the sunny-side-up drops because the liquid film filling the interstice of the micro-pattern closes up with the plane top faces of the post.
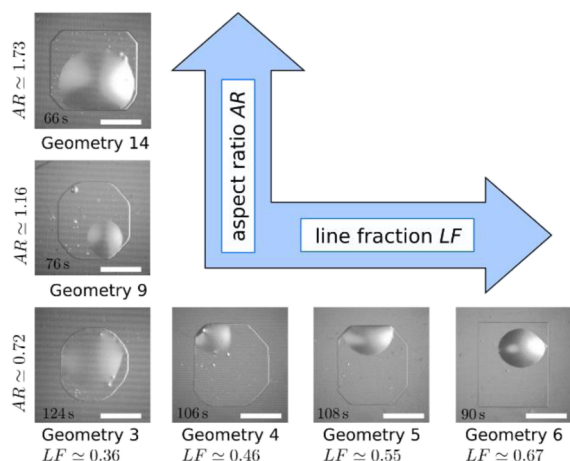
FIG. 5. Shapes of sunny-side-up drops on pattern geometries of triangular posts with similar line aspect ratios and increasing line fractions (horizontal direction), as well as with similar line fractions and increasing aspect ratios (vertical direction).

Hence, the liquid interface of the film can be thought of as a plane but chemically patterned surface with a zero material contact angle on the film and a finite material contact angle on the top surfaces of the posts. In the present situation, the Cassie model predicts an increase in the apparent contact angle of the egg-yolk drop with an increasing post density,[30,31] but no dependence on the aspect ratio of the posts.

3. Late time

In the late stage of evaporation, only a short time before all liquid has evaporated, we observe a retraction of the film edge in the micro-pattern from its initial position immediately after deposition. On geometries with dense post arrays, this receding motion leads to highly irregular contours of the residual film, which can be seen, e.g., in the last image of the time series on pattern geometries 3–6 in Fig. 2. Notably, the optical contrast of the wicking film at this point has changed as compared to the contrast in the presence of an egg-yolk drop. This change of contrast can be related to the mean curvature of the liquid–air interface evolving from a positive value close to zero in the sunny-side-up state to negative before the film edge starts to retract.

A clear dependence of the onset of retraction on the orientation of the film edge could not be detected in our experiments. Inspection of the last image in the time series shown in Fig. 2 shows that the corrugation of the retracting film contour in the late time regime correlates with the geometry of the micro-pattern, being most pronounced on surfaces with dense arrays of low aspect ratio posts. However, the contours of the retracting film edge on pattern geometries with high aspect ratio posts are irregular but smoother as compared to the films at late times on geometries with low aspect ratio posts.

4. Evolution classes

Based on the sequence of drop morphologies in Fig. 2, we can group the tested pattern geometries according to the evolution of drop shapes observed during evaporation. In the following, we will

distinguish four different classes of drop evolution according to the features observed during early, intermediate, and late times.

The first class comprises pattern geometries with drops that remain in the Wenzel state. Drops wetting this class of pattern geometry display a circular drop base during the entire evaporation process and are found predominantly on geometries with a small line fraction or low aspect ratio. Pattern geometries with Wenzel drops are labeled with a filled circle.

On the remaining tested pattern geometries, we observed directional pinning of the interface into the lattice directions of the micro-pattern and, on some of the geometries, also pinning into the respective diagonal directions. Because of the strong interfacial pinning, drops on these patterns retain the shape of their initial footprint after deposition and transform into a sunny-side-up drop with a homogeneous wicking film around the drop base. Depending on the shape of the drop's footprint, we distinguish between pattern geometries with sunny-side-up drops of circular footprint (open circle symbol), octagonal footprint (plus/octagon symbol), and rectangular or mixed octagonal/rectangular footprint (square symbol).

B. Numerical results

To understand the shape evolution of evaporating drops in relation to the predicted stability of liquid films wicking the micro-pattern, we will first provide the reader with a review of our numerical results that were previously published in Ref. 20. We will continue with a discussion of the conditions to observe receding films at different orientations of the film edge relative to the micro-pattern of triangular posts.

1. Film edge morphology and stability

Two locally stable interface morphologies of the terminal region of the liquid film are found in our numerical model for the condition of zero Laplace pressure, a material contact angle of $\theta = 50°$,[20] and for a given orientation of the film edge to the lattice directions. Owing to the discrete symmetries of the micro-pattern, we distinguish between only three different orientations of the film edge relative to the posts.

Examples for the two morphologies of the terminal meniscus of the film edge are shown in Fig. 6 and illustrate the characteristic features of the two morphologies for the example of the side orientation. The terminal three-phase contact line of the pinned meniscus morphology is located on the bottom surface and the side faces of the posts, cf. Fig. 6(a). In contrast to the pinned meniscus morphology, the entire terminal three-phase contact line of the coalesced meniscus morphology shown in Fig. 6(b) is located on the bottom part of the surface. Both meniscus morphologies are also found for film edges in tip-orientation and in base-orientation, i.e., with the tips of the triangles pointing out of, respectively, into the film.

For a given orientation of the film edge relative to the array of posts, both stable morphologies are restricted to pattern geometries within a certain range of line fractions and aspect ratios of the triangular posts. The stability is illustrated best in the form of a stability diagram in terms of the line fraction LF and aspect ratio AR. Each point (LF, AR) representing a pair of control parameters is assigned to the coalesced or pinned meniscus morphologies, provided this morphology exists as a local minimum of the interfacial
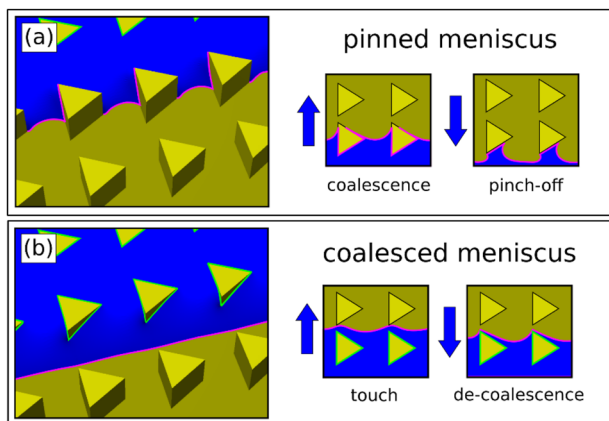
FIG. 6. *Left*: Renderings of (a) the pinned meniscus morphology and (b) the coalesced meniscus morphology found in our numerical energy minimization for a film edge in side-orientation. *Right*: Illustrations of capillary instabilities for an advancing and a receding film delimiting the stable region of the respective meniscus morphology. The terminal three-phase contact line is shown in magenta, while the contacts line wrapping around the post is highlighted in green.

energy for the given control parameters. Stability diagrams for the coalesced and the pinned meniscus derived from our numerical energy minimizations are shown in Fig. 7 for a film edge in (a) tip-orientation, (b) base-orientation, and (c) side-orientation. Note that both meniscus morphologies can be stable on the same pattern geometry.

Because every region of line fractions and aspect ratios corresponds to pattern geometries on which certain meniscus morphologies are found as stable interfacial shapes, each point on the boundary of that region must be related to a specific interfacial instability of the respective meniscus morphology. The interfacial instabilities of the pinned meniscus morphology and the coalesced meniscus morphology are shown in Figs. 6(a) and 6(b), respectively.

Considering the instabilities of the pinned meniscus morphology, we find a coalescence of the terminal meniscus ahead of the posts for dense and high aspect ratio posts and a pinch-off of the wetting liquid from the rear of the posts if the posts are too sparse or if their aspect ratio is too low. As a result of the coalescence, the contact lines of the coalesced meniscus morphology in the terminal row fully wrap around the posts, cf. Fig. 6(a). The coalesced meniscus morphology formed because of the coalescence or pinch-off instability may represent a local energy minimum or a transient interface configuration.

For the coalesced meniscus morphology, the liquid meniscus in the last row of posts in contact with the film may break up, or "de-coalesce," into the pinned meniscus morphology whenever the spacing of the posts is too sparse or the aspect ratio too low, cf. Fig. 6(b). On the contrary, if the spacing of the post is too close or the aspect ratio is too high, the terminal contact line touches the next row of dry posts ahead of the terminal meniscus, leading to the formation of a pinned meniscus morphology. The pinned meniscus formed because of the de-coalescence or touch instability may represent a local energy minimum or a transient interface configuration.

A retraction of the liquid film is possible only if the pinned morphology of the film edge can detach from the posts and, at the same time, the coalesced morphology of the film edge can recede after spontaneous de-coalescence of the liquid ahead of the posts. A spontaneous progression or retraction of the film edge can occur only in those regions of control parameters (LF, AF) where neither the stable coalesced meniscus nor the stable pinned meniscus morphology exists.[20,24] Here, our numerical model predicts that the edge of the film cannot be arrested in the micro-pattern and recedes if the line fraction and aspect ratio fall into the de-wicking region located below both the pinch-off instability line and the de-coalescence instability line. The de-wicking region is shown as the blue area in the stability diagrams in Figs. 7(a)–7(c).

A close inspection of the stability diagrams for all three orientations of the film edge Figs. 7(a)–7(c) reveals that the line limiting the region of pattern geometries with stable pinned meniscus morphologies toward a pinch-off is located at lower line fractions and aspect ratios as compared to the instability line limiting the region of pattern geometries with stable coalesced meniscus morphologies toward de-coalescence. Hence, we conclude that the pinch-off of the pinned meniscus morphology represents the ultimate interfacial instability, defining the range of stable film edges toward low line fractions or low aspect ratios for all three orientations considered. The pinch-off, thus, determines whether a liquid film spontaneously recedes from the micro-pattern or whether the edge of the film is arrested.

C. Comparison to stability diagram

To relate the observed evolution of drop morphologies to the stability of the terminal meniscus of the film edge at different orientations, we map the line fraction $LF = w/d$ and aspect ratio $AR = h/w$ of the pattern geometries corresponding to a certain class of drop shape evolution into the numerically determined stability diagram of the terminal meniscus shown in Figs. 7(a)–7(c). Here, we show only the ultimate stability boundaries of the pinned and coalesced meniscus morphologies to keep the emerging stability diagram in Fig. 8 concise. Since we want to assess a potential directional dependence, we still distinguish between a film edge in tip-orientation, side-orientation, and in base-orientation. Symbols indicating the four different types of morphological evolution of evaporation drops observed on the pattern geometries are described in Sec. III A and are identical to those in Fig. 2.

As mentioned earlier in Sec. III A, the region of a de-wicking film in the numerically determined stability diagram is limited by the pinch-off instability of the pinned meniscus morphology for all three orientations of the film edge considered here. Hence, the pinch-off instability line bounds the region in the stability diagram in Fig. 8 where spontaneous de-wicking can occur toward large aspect ratios and large line fractions. The boundary curves related to the pinch-off instability of the pinned meniscus morphology are very similar for a film edge in tip-orientation, in base-orientation, and in side-orientation, cf. also Fig. 8.

The edge of a wicking film is immobilized in micro-patterns with sufficiently large line fractions and aspect ratios because the terminal meniscus at the film edge in the pinned morphology cannot detach from the posts. This finding is in full agreement with our general experimental finding that the mobility of the interface in contact
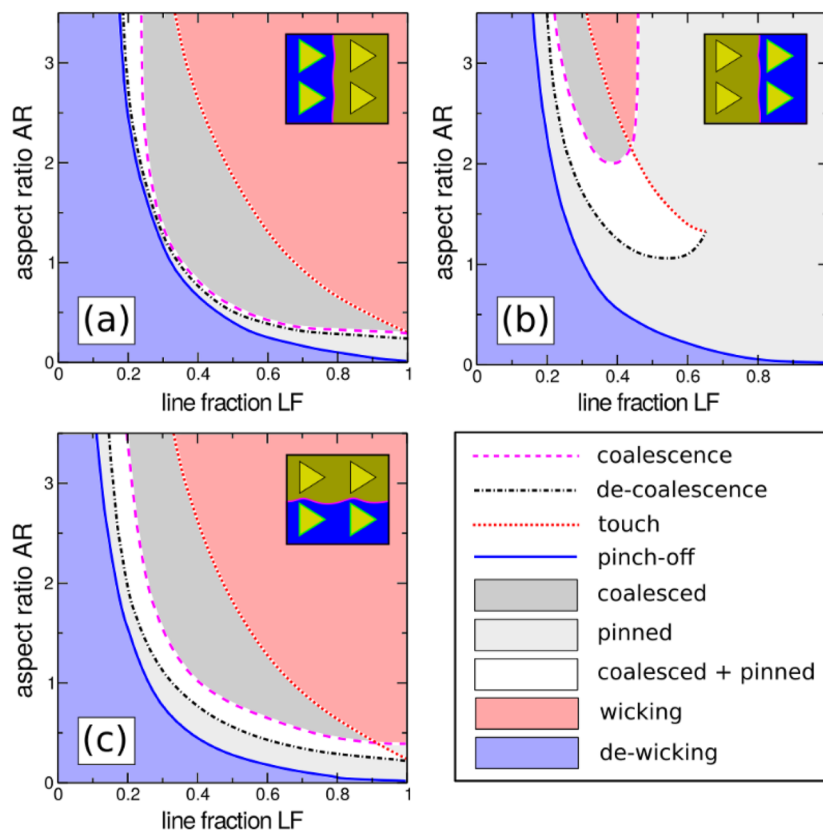
FIG. 7. (a)–(c): Pattern geometries with line fraction $LF = w/d$ and aspect ratio $AR = h/w$ of the posts on which the coalesced meniscus morphology (dark gray), the pinned meniscus morphology (light gray), or both meniscus morphologies (white) are local minima of the interfacial energy for a material contact angle of $\theta = 50°$. Shown are stability diagrams for terminal menisci of a film edge in (a) tip-orientation, (b) in base-orientation, and (c) in side-orientation. Regions where neither of the two meniscus morphologies exists correspond to an advancing (red) or a receding (blue) liquid film. Different instabilities that make up the boundaries of the stable regions are distinguished by different line styles.

with the pattern geometries investigated in this study is governed by the line fraction and aspect ratio of the triangular posts and is not sensitive to the orientation of the film edge with respect to the direction of the triangular posts.

Consistent with the predictions of the numerical model for a contact angle of $\theta = 50°$, we find that the Wenzel drops on surface geometries 1, 2, and 7 fall into the region of line fractions and aspect ratios where spontaneous de-wicking in all orientations of the film edge is predicted for the pattern geometries and, hence, cannot shed a wicking film during evaporation. Because the shape of the Wenzel drops remains close to a spherical cap during evaporation, the receding contact angle of the drop's interface cannot depend on the orientation of the interface relative to the pattern.

In terms of the line fraction and aspect ratio of posts, pattern geometries 12 and 15b are located close to the pinch-off instability line and display spherical cap-shaped drops with an almost uniformly shrinking footprint. The discrepancy between Wenzel drops on geometry 15b and with a pinned drop base on geometry 15a could be explained through unavoidable imperfections during sample preparation and points to a high sensitivity of the contact line

mobility with respect to the geometry of the micro-pattern in that region of the parameter space.

Line fractions and aspect ratios of pattern geometries where sunny-side-up drops are observed fall in the region of the stability diagram in Fig. 8, where the pinned meniscus morphology represents a local minimum of the interfacial energy. All pattern geometries where drops with a pinned angular or circular footprint are observed map into the region where the numerical model predicts stable pinned menisci. The line fractions and aspect ratios of micro-patterns on geometries 6 and 10 where the drops' footprints display an overall rectangular shape are the closest to the line bounding the region of spontaneous wicking in the stability diagram Fig. 8.

Generally, we observe the tendency of the film enclosing the drop to become less isotropic and to form fewer facets if the pattern geometry is closer to the wicking region in the stability diagram in Fig. 8 in terms of line fraction and aspect ratio. A similar sequence of polygonal film shapes becoming less isotropic has been noted in Ref. 11 for drops wicking a square lattice of circular posts. Different from our study, the transition from circular over octagonal to
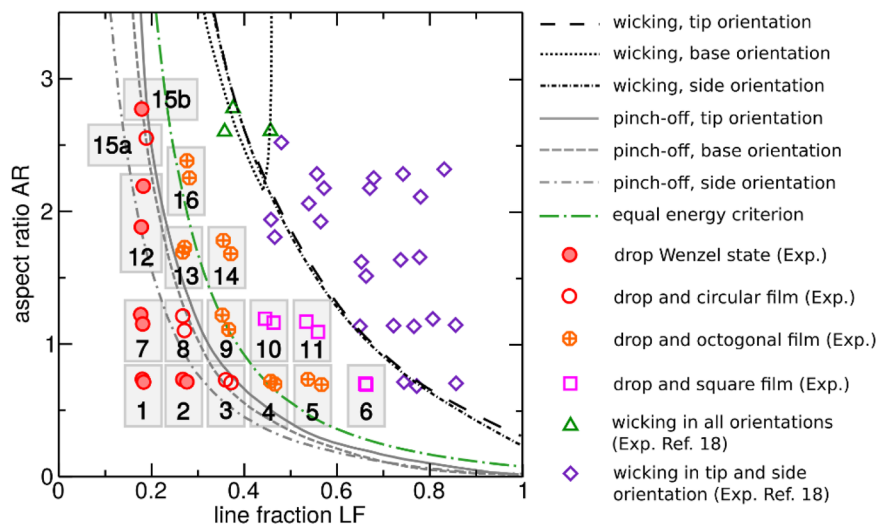
FIG. 8. Stability diagram of the terminal meniscus for different orientations of the film edge and observed the wicking and de-wicking of heptane drops on micro-patterned surfaces with different line fractions $LF = w/d$ and aspect ratios $AR = h/w$ for a material contact angle of $\theta = 50°$. Symbols indicate the four morphological evolutions observed on the tested geometries, cf. also Figs. 2 and 3.

a square film contour has been related in Ref. 11 to a decrease in the surface energy driving the wicking, which leads to a decreasing velocity of the advancing film.

IV. CONCLUSIONS AND OUTLOOK

This work shows that the region of line fractions and aspect ratios where stable films are observed on an anisotropic micro-pattern of triangular posts during evaporation conforms to predictions of our numerical model, complementing the former study of spontaneous wicking with data on spontaneous retraction of a liquid film. In contrast to previous experiments on spontaneous wicking, the experimental results reported in this work demonstrate that the interface mobility of heptane drops de-wetting from a micro-pattern of posts with a triangular cross section does not break the symmetry of the rectangular post lattice. A contact line mobility independent of the orientation of the three-phase contact line is observed on geometries with sparse or flat triangular posts, leading to uniformly shrinking spherical cap-shaped Wenzel drops.

Our study confirms that drops on micro-patterns with dense and tall triangular posts eventually evolve into sunny-side-up drops during evaporation. In terms of the control parameters line fraction and aspect ratio of the micro-pattern geometry, the boundary line delimiting the regions of Wenzel drops from regions of sunny-side-up drops conforms well to the numerically determined pinch-off instability of the terminal film meniscus for a material contact angle of $50°$. The insensitivity of the pinch-off instability with respect to the orientation of the film edge explains why the shape of the film does not break the symmetry of the post lattice despite the triangular cross-section of the posts.

Most strikingly, we did not observe any coherently receding film edge in our experiments during evaporation. This may be the case for two reasons: First, any observable liquid film has already retracted fully into the drop base of Wenzel drops shortly after deposition. Second, the receding film edge observed at the end of the sunny-side-up state always evolves into an irregular shape. To learn more about the mobility of receding wicking films and about the dynamics of interfaces on micro-patterned surfaces, in general, it would be interesting to observe the mobility of transient menisci at different orientations of the film edge with a high-speed camera shortly after the impact of a liquid drop on the surface.

SUPPLEMENTARY MATERIAL

See the supplementary material for a table of measured dimensions of the pattern geometries used in de-wetting experiments.

AUTHOR DECLARATIONS

Conflict of Interest

The authors have no conflicts to disclose.

Author Contributions

Hsuan-Yi Peng: Investigation (equal); Writing – original draft (equal); Writing – review & editing (equal). **Bang-Yan Liu**: Investigation (equal); Writing – original draft (equal); Writing – review &

editing (equal). **Chi-Chun Lo**: Investigation (equal); Writing – original draft (equal); Writing – review & editing (equal). **Li-Jen Chen**: Investigation (equal); Writing – original draft (equal); Writing – review & editing (equal). **Ralf Seemann**: Investigation (equal); Writing – original draft (equal); Writing – review & editing (equal). **Martin Brinkmann**: Investigation (equal); Writing – original draft (equal); Writing – review & editing (equal).

DATA AVAILABILITY

The data that support the findings of this study are available within the article and its supplementary material.

REFERENCES

[1]M. Alava, M. Dubé, and M. Rost, "Imbibition in disordered media," Adv. Phys. **53**, 83–175 (2004).

[2]J. Ha, J. Kim, Y. Jung, G. Yun, D.-N. Kim, and H.-Y. Kim, "Poro-elastocapillary wicking of cellulose sponges," Sci. Adv. **4**, eaa07051 (2018).

[3]Z. Liu, X. He, J. Han, X. Zhang, F. Li, A. Li, Z. Qu, and F. Xu, "Liquid wicking behavior in paper-like materials: Mathematical models and their emerging biomedical applications," Microfluid. Nanofluid. **22**, 132 (2018).

[4]A. Nikolov, S. Murad, D. Wasan, and P. Wu, "How the capillarity and ink-air flow govern the performance of a fountain pen," J. Colloid Interface Sci. **578**, 660–667 (2020).

[5]D. Bonn, J. Eggers, J. Indekeu, J. Meunier, and E. Rolley, "Wetting and spreading," Rev. Mod. Phys. **81**, 739–805 (2009).

[6]G. McHale, N. J. Shirtcliffe, and M. I. Newton, "Super-hydrophobic and super-wetting surfaces: Analytical potential?," Analyst **129**, 284 (2004).

[7]D. Quéré, "Non-sticking drops," Rep. Prog. Phys. **68**, 2495–2532 (2005).

[8]A. D. Dussaud, P. M. Adler, and A. Lips, "Liquid transport in the networked microchannels of the skin surface," Langmuir **19**, 7341–7345 (2003).

[9]P. Ge, S. Wang, J. Zhang, and B. Yang, "Micro-/nanostructures meet anisotropic wetting: From preparation methods to applications," Mater. Horiz. **7**, 2566–2595 (2020).

[10]C. Ishino, M. Reyssat, E. Reyssat, K. Okumura, and D. Quéré, "Wicking within forests of micropillars," Europhys. Lett. **79**, 56005 (2007).

[11]L. Courbin, E. Denieul, E. Dressaire, M. Roper, A. Ajdari, and H. A. Stone, "Imbibition by polygonal spreading on micro- decorated surfaces," Nat. Mater. **6**, 661–664 (2007).

[12]L. Courbin, J. C. Bird, M. Reyssat, and H. A. Stone, "Dynamics of wetting: From inertial spreading to viscous imbibition," J. Phys.: Condens. Matter **21**, 464127 (2009).

[13]Q. Yuan and Y.-P. Zhao, "Multiscale dynamic wetting of a droplet on a lyophilic pillar-arrayed surface," J. Fluid Mech. **716**, 171–188 (2013).

[14]K.-H. Chu, R. Xiao, and E. N. Wang, "Uni-directional liquid spreading on asymmetric nanostructured surfaces," Nat. Mater. **9**, 413–417 (2010).

[15]J. Feng and J. P. Rothstein, "One-way wicking in open micro-channels controlled by channel topography," J. Colloid Interface Sci. **404**, 169–178 (2013).

[16]C. Sammartino, M. Rennick, H. Kusumaatmaja, and B.-E. Pinchasik, "Three-dimensional printed liquid diodes with tunable velocity: Design guidelines and applications for liquid collection and transport," Phys. Fluids **34**, 112113 (2022).

[17]C. Q. Lai, C. V. Thompson, and W. K. Choi, "Uni-, bi-, and tri-directional wetting caused by nanostructures with anisotropic surface energies," Langmuir **28**, 11048–11055 (2012).

[18]V. Jokinen, "Directional imbibition on a chemically patterned silicon micropillar array," Soft Matter **12**, 1100–1106 (2016).

[19]V. Jokinen, M. Leinikka, and S. Franssila, "Microstructured surfaces for directional wetting," Adv. Mater. **21**, 4835–4838 (2009).

[20]B.-Y. Liu, L.-J. Chen, R. Seemann, and M. Brinkmann, "Directional liquid wicking in regular arrays of triangular posts," Langmuir **35**, 16476–16486 (2019).

[21]M. L. Blow, H. Kusumaatmaja, and J. M. Yeomans, "Imbibition through an array of triangular posts," J. Phys.: Condens. Matter **21**, 464125 (2009).

[22]M. L. Blow and J. M. Yeomans, "Anisotropic imbibition on surfaces patterned with polygonal posts," Philos. Trans. R. Soc., A **369**, 2519–2527 (2011).

[23]P. Comanns, G. Buchberger, A. Buchsbaum, R. Baumgartner, A. Kogler, S. Bauer, and W. Baumgartner, "Directional, passive liquid transport: The Texas horned lizard as a model for a biomimetic 'liquid diode,'" J. R. Soc., Interface **12**, 20150415 (2015).

[24]C. Semprebon, P. Forsberg, C. Priest, and M. Brinkmann, "Pinning and wicking in regular pillar arrays," Soft Matter **10**, 5739–5748 (2014).

[25]K.-Y. Law and H. Zhao, "Contact angle measurements and surface characterization techniques," in *Surface Wetting* (Springer, Cham, 2015), pp. 7–34.

[26]K.-Y. Yeh, K.-H. Cho, Y.-H. Yeh, A. Promraksa, C.-H. Huang, C.-C. Hsu, and L.-J. Chen, "Observation of the rose petal effect over single- and dual-scale roughness surfaces," Nanotechnology **25**, 345303 (2014).

[27]K. A. Brakke, "The surface evolver," Exp. Math. **1**, 141–165 (1992).

[28]P. S. H. Forsberg, C. Priest, M. Brinkmann, R. Sedev, and J. Ralston, "Contact line pinning on microstructured surfaces for liquids in the Wenzel state," Langmuir **26**, 860–865 (2010).

[29]C. Ishino and K. Okumura, "Wetting transitions on textured hydrophilic surfaces," Eur. Phys. J. E **25**, 415–424 (2008).

[30]A. B. D. Cassie, "Contact angle," Discuss. Faraday Soc. **3**, 11–16 (1948).

[31]C. Priest, R. Sedev, and J. Ralston, "Asymmetric wetting hysteresis on chemical defects," Phys. Rev. Lett. **99**, 026103 (2007).